

Plasma-wave interaction in helicon plasmas near the lower hybrid frequency

Yide Zhao(赵以德), Jinwei Bai(白进纬), Yong Cao(曹勇), Siyu Wu(吴思宇), Eduardo Ahedo, Mario Merino, and Bin Tian(田滨)

Citation: Chin. Phys. B, 2022, 31 (**7**): 075203. DOI: 10.1088/1674-1056/ac40fd
Journal homepage: http://cpb.iphy.ac.cn; http://iopscience.iop.org/cpb

What follows is a list of articles you may be interested in

Influence of oxygen addition on the discharge characteristics of an argon plasma jet at atmospheric pressure

Junyu Chen(陈俊宇), Na Zhao(赵娜), Jiacun Wu(武珈存), Kaiyue Wu(吴凯玥), Furong Zhang(张芙蓉),Junxia Ran(冉俊霞), Pengying Jia(贾鹏英), Xuexia Pang(庞学霞), and Xuechen Li(李雪辰)

Chin. Phys. B, 2022, 31 (**6**): 065205. DOI: 10.1088/1674-1056/ac601a

Spatial characteristics of nanosecond pulsed micro-discharges in atmospheric pressure He/H_2O mixture by optical emission spectroscopy

Chuanjie Chen(陈传杰), Zhongqing Fang(方忠庆), Xiaofang Yang(杨晓芳), Yongsheng Fan(樊永胜), Feng Zhou(周锋), and Rugang Wang(王如刚)

Chin. Phys. B, 2022, 31 (**2**): 025204. DOI: 10.1088/1674-1056/ac2e62

Numerical investigation of radio-frequency negative hydrogen ion sources by a three-dimensional fluid model

Ying-Jie Wang(王英杰), Jia-Wei Huang(黄佳伟), Quan-Zhi Zhang(张权治), Yu-Ru Zhang(张钰如), Fei Gao(高飞), and You-Nian Wang(王友年)

Chin. Phys. B, 2021, 30 (**9**): 095205. DOI: 10.1088/1674-1056/ac0e21

Optimized calculation of the synergy conditions between electron cyclotron current drive and lower hybrid current drive on EAST

Wei Wei(韦维), Bo-Jiang Ding(丁伯江), Y Peysson, J Decker, Miao-Hui Li(李妙辉),Xin-Jun Zhang(张新军), Xiao-Jie Wang(王晓洁), Lei Zhang(张磊)

Chin. Phys. B, 2016, 25 (**1**): 015201. DOI: 10.1088/1674-1056/25/1/015201

Reconstruction of heat flux profile on the HL-2A divertor plate with a three-dimensional analysis model

Gao Jin-Ming, Li Wei, Xia Zhi-Wei, Pan Yu-Dong, Lu Jie, Yi Ping, Liu Yi

Chin. Phys. B, 2013, 22 (**1**): 015202. DOI: 10.1088/1674-1056/22/1/015202

Plasma–wave interaction in helicon plasmas near the lower hybrid frequency

Yide Zhao(赵以德)[1], Jinwei Bai(白进纬)[2], Yong Cao(曹勇)[2], Siyu Wu(吴思宇)[2], Eduardo Ahedo[3], Mario Merino[3], and Bin Tian(田滨)[2,†]

[1] *Science and Technology on Vacuum Technology and Physics Laboratory, Lanzhou Institute of Physics, Lanzhou* 730000, *China*
[2] *School of Mechanical Engineering and Automation, Harbin Institute of Technology, Shenzhen* 518055, *China*
[3] *Equipo de Propulsión Espacial y Plasmas (EP2), Universidad Carlos III de Madrid,* 28911 *Leganés, Spain*

(Received 16 September 2021; revised manuscript received 6 December 2021; accepted manuscript online 8 December 2021)

We study the characteristics of plasma–wave interaction in helicon plasmas near the lower hybrid frequency. The (0D) dispersion relation is derived to analyze the properties of the wave propagation and a 1D cylindrical plasma–wave interaction model is established to investigate the power deposition and to implement the parametric analysis. It is concluded that the lower hybrid resonance is the main mechanism of the power deposition in helicon plasmas when the RF frequency is near the lower hybrid frequency and the power deposition mainly concentrates on a very thin layer near the boundary. Therefore, it causes that the plasma resistance has a large local peak near the lower hybrid frequency and the variation of the plasma density and the parallel wavenumber lead to the frequency shifting of the local peaks. It is found that the magnetic field is still proportional to the plasma density for the local maximum plasma resistance and the slope changes due to the transition.

Keywords: helicon plasmas, lower hybrid frequency, power deposition

PACS: 52.50.Dg, 52.50.Qt **DOI:** 10.1088/1674-1056/ac40fd

1. Introduction

Helicon waves propagating near lower hybrid frequencies in plasmas have been significantly studied since the 1970s.[1,2] It plays an important role in space plasmas and fusion research due to the close relation to the ion heating and the lower-hybrid drift instability.[3–5] In the 1980s, the investigation of influence of lower hybrid frequencies in plasma discharges was studied by Boswell and Zhu.[6,7] They found that a very dense plasma can be produced near lower hybrid frequencies with helicon waves. After that, the extensive studies on lower hybrid frequencies for the helicon discharge were carried out by many researchers.[8–11]

The lower hybrid frequency $\omega_{\rm lh}$ is a resonant frequency between the electron cyclotron frequency $\omega_{\rm ce}$ and the ion cyclotron frequency $\omega_{\rm ci}$ and has the following form:[12]

$$\omega_{\rm lh} = \left[\frac{1}{\omega_{\rm ci}\omega_{\rm ce}} + \frac{1}{\omega_{\rm pi}^2 + \omega_{\rm ci}^2}\right]^{-1/2} \approx \sqrt{\omega_{\rm ci}\omega_{\rm ce}}, \qquad (1)$$

where $\omega_{\rm pi}$ represents the ion plasma frequency. Near the lower hybrid frequency, the effect of ion motion cannot be neglected. The basic wave theory shows that the resonance occurs when the frequency reaches $\omega_{\rm lh}$.[13] It is expected to be beneficial for the power deposition. The experimental results by Yun *et al.*[8,14] confirmed this prediction. They tested the frequency dependence of helicon plasmas for different magnetic fields and various gases. It was shown that the optimum frequency yielding the highest plasma density is near the lower hybrid frequency and it was suggested that the lower hybrid resonance heating may be important in helicon sources.[8] However, the optimum frequency is not exactly equal to $\omega_{\rm lh}$ but slightly lower. This may be explained by the Doppler shift effect.[8]

In order to study the role of the lower hybrid frequency in helicon discharges, Cho gave the self-consistent results coupling the wave equations to the global balance equations.[13] He found that there are many eigenmodes when the operation frequency is higher than $\omega_{\rm lh}$, but there are only a few isolated eigenmodes for frequencies lower than $\omega_{\rm lh}$. Furthermore, an eigenmode always exists near the lower hybrid frequency. This behavior leads to the variation of the resistance with the frequency. Specifically, the self-consistent results show that the abrupt density jump occurs near the lower hybrid frequency. These conclusions were also confirmed in the experiments by Kwak *et al.*[15] Moreover, in the study of the instabilities and anisotropy in the hot-helicon experimental device (HELIX), Scime *et al.*[16] found that there is a clear increase in electron temperature as the antenna frequency is near the lower hybrid frequency. Additional experimental results obtained by Balkey *et al.*[10] indicated that the maximum electron density is measured when the rf frequency is near the lower hybrid frequency. It is consistent with the previous results by others. However, the maximum ion temperature is measured when $\omega < 0.7\omega_{\rm lh}$. It is suggested that the mechanism of power deposition for ions and electrons in helicon

†Corresponding author. E-mail: tianbin@hit.edu.cn

© 2022 Chinese Physical Society and IOP Publishing Ltd

sources is distinct. When studying very light ion mass gases such as hydrogen, Mori *et al.*[11] found that the optimal frequency can be away from $\omega_{\rm lh}$ in a non-uniform magnetic field as long as the RF power is large enough. In addition, the experiments by Buttenschon *et al.*[17] showed that the linear scaling of the plasma density with magnetic fields can be observed in the frequency range of $\omega_{\rm lh} \leq 0.8\omega$.

Therefore, the lower hybrid frequency and its resonance occurring plays a vital role in helicon plasmas. However, the influence of the parameters on the lower hybrid resonance has not been fully studied. In this paper, a detailed (0D) dispersion relation of helicon plasmas is derived to investigate the characteristics of wave propagation and the power deposition near the lower hybrid frequency. A 1D cylindrical plasma–wave interaction model is established to study the wave property and the parametric investigations are carried out to analyze the influence of the applied magnetic fields, plasma density and RF frequency on the helicon plasmas.

The structure of this paper is as follows. The basic theory is implemented in Section 2. Section 3 presents the simulation results and discussion. The conclusion is given in Section 4.

2. Theory

2.1. The (0D) dispersion relation

In order to analyze the plasma–wave interaction near the lower hybrid frequency, the dispersion relation is discussed in detail. In a magnetized plasma, the general dispersion relation is very complicated. To understand the wave properties, we limit the study to linear waves, of single frequency ω propagating into a plasma where an axially stationary magnetic field $\boldsymbol{B}_0$ is applied. The plasma–wave response is assumed to vary as $\exp(\mathrm{i}\boldsymbol{k}\cdot\boldsymbol{r} - \mathrm{i}\omega t)$ and is governed by the Maxwell equations:

$$\nabla \times \boldsymbol{E} = \mathrm{i}\omega\boldsymbol{B}, \tag{2}$$

$$\nabla \times \boldsymbol{B} = \mu_0(-\mathrm{i}\omega\overline{\overline{\varepsilon}}\cdot\boldsymbol{E} + \boldsymbol{j}_{\rm a}), \tag{3}$$

where $\boldsymbol{E}$ and $\boldsymbol{B}$ represent only the RF-related electromagnetic field, $\boldsymbol{j}_{\rm a}$ is the external current density from the antenna. Fourier expansion in time has been applied, and all magnitudes are expressed in complex form. In addition, $\overline{\overline{\varepsilon}}$ is the plasma dielectric tensor. For a cold weakly collisional plasma, it takes the form[18]

$$\overline{\overline{\varepsilon}} = \varepsilon_0 \begin{bmatrix} \kappa_1 & \mathrm{i}\kappa_2 & 0 \\ -\mathrm{i}\kappa_2 & \kappa_1 & 0 \\ 0 & 0 & \kappa_3 \end{bmatrix} \tag{4}$$

with the elements

$$\kappa_1 = 1 - \sum_j \frac{\omega_{{\rm p}j}^2(\omega + \mathrm{i}\nu_j)}{\omega\left[(\omega+\mathrm{i}\nu_j)^2 - \omega_{{\rm c}j}^2\right]}, \tag{5}$$

$$\kappa_2 = -\sum_j \frac{s_j\omega_{{\rm c}j}\omega_{{\rm p}j}^2}{\omega\left[(\omega+\mathrm{i}\nu_j)^2 - \omega_{{\rm c}j}^2\right]}, \tag{6}$$

$$\kappa_3 = 1 - \sum_j \frac{\omega_{{\rm p}j}^2}{\omega(\omega+\mathrm{i}\nu_j)}, \tag{7}$$

where $\omega_{{\rm c}j}$ and $\omega_{{\rm p}j}$ are the cyclotron and electrostatic frequencies (of species $j = \mathrm{i}, \mathrm{e}$), ν_j is the collision frequency and s_j is the sign of the electric charge. When the emission frequency is near the lower hybrid frequency, the influence of ions on the plasma–wave interaction cannot be neglected. The ion mass has to be taken into account in the dieletric tensor. Simplifying Eqs. (2) and (3), the dispersion relation in helicon plasmas can be written in a biquadratic form[18]

$$aK^4 + bK^2 + d = 0. \tag{8}$$

Here, we introduce the normalized parameter $K = kd_{\rm e}$, with the wavenumber k, the electron skin depth $d_{\rm e} = c/\omega_{\rm pe}$ and the light speed in vacuum c. This non-dimensional parameter includes the influence of the wavenumber k and the electron density $n_{\rm e}$. It is convenient to carry out the parametric analysis. In addition, a, b and d are coefficients related to the dielectric tensor components

$$\begin{aligned} a &= \hat{\kappa}_1\sin^2\theta + \hat{\kappa}_3\cos^2\theta, \\ b &= \left(\hat{\kappa}_2^2 - \hat{\kappa}_1^2\right)\sin^2\theta - \hat{\kappa}_1\hat{\kappa}_3(1+\cos^2\theta), \\ d &= \left(\hat{\kappa}_1^2 - \hat{\kappa}_3^2\right), \end{aligned} \tag{9}$$

where θ is the angle between $\boldsymbol{B}_0$ and $\boldsymbol{k}$. Parallel and perpendicular wavenumbers are defined as $k_\parallel = k\cos\theta$ and $k_\perp = k\sin\theta$. Also, the normalized element of dieletric tensor is

$$\hat{\kappa}_j = \kappa_j\frac{\omega^2}{\omega_{\rm pe}^2}.$$

To solve this dispersion relation, the basic characteristics of helicon waves can be analyzed. Two pairs of solutions for this biquadratic equation represent two branches of waves, named as the helicon (HE) mode and the Trivelpiece–Gould (TG) mode.[19] The helicon mode is an electromagnetic wave with long wavelength. In contrast, the TG mode is an electrostatic wave and has a larger perpendicular wavenumber $k_\perp$ than the helicon mode, hence shorter wavelength is achieved.

2.2. The 1D plasma–wave interaction model

In this section, the 1D cylindrical model available is established to investigate the plasma–wave interaction in helicon plasmas. Based on the assumption in the derivation of the dispersion relation, more conditions due to the geometry and practice are taken into account. We consider a cylindrical source of length L and radius $r_{\rm p}$ filled with a fully ionized plasma. The radial variation of the plasma density, $n = n(r)$, is known. The plasma source is surrounded by an antenna, which is assumed to be infinitely thin and located at $r = r_{\rm a}$,

with $r_a > r_p$. The plasma is confined radially by the applied axial magnetic field B_0, created by a set of external coils (which are assumed to have no effects on the plasma–wave interaction). The whole set is immersed in a larger conducting vessel of length L and radius r_w with $r_w > r_a$.

For a finite length cylinder source, the plasma is bounded by conducting plates at both ends. Therefore, the reflection boundary conditions are achieved at the two conducting end walls. Then, the components of EM fields can be expanded in the following (z,θ) Fourier series,[20]

$$\begin{aligned}&\begin{pmatrix}E_r(r,\theta,z,t)\\E_\theta(r,\theta,z,t)\\B_z(r,\theta,z,t)\end{pmatrix}\\&=\sum_{l,m}\begin{pmatrix}E_r^{(l,m)}(r)\\E_\theta^{(l,m)}(r)\\B_z^{(l,m)}(r)\end{pmatrix}\sin\left(\frac{l\pi}{L}z\right)\exp\left[\mathrm{i}\left(m\theta-\omega t\right)\right],\end{aligned}\tag{10}$$

$$\begin{aligned}&\begin{pmatrix}B_r(r,\theta,z,t)\\B_\theta(r,\theta,z,t)\\E_z(r,\theta,z,t)\end{pmatrix}\\&=\sum_{l,m}\begin{pmatrix}B_r^{(l,m)}(r)\\B_\theta^{(l,m)}(r)\\E_z^{(l,m)}(r)\end{pmatrix}\cos\left(\frac{l\pi}{L}z\right)\exp\left[\mathrm{i}\left(m\theta-\omega t\right)\right],\end{aligned}\tag{11}$$

where $k_\parallel = k_l = l\pi/L$ is the parallel wavenumber; m is integer, and l is natural.

Considering the geometry of the antenna, the general form of the current density is

$$\begin{aligned}\boldsymbol{j}_a(\boldsymbol{r},t) &= I_a\delta(r-r_a)\left[1_z s_z(\theta,z)+1_\theta s_\theta(\theta,z)\right]\\&\quad\times\exp(-\mathrm{i}\omega t),\end{aligned}\tag{12}$$

where I_a is the antenna current; s_z and s_θ define the linear shape of the antenna.[21] This current density is also expanded as

$$j_\theta(r,\theta,z,t)=\sum_{m,l}j_\theta^{(l,m)}(r)\sin\left(\frac{l\pi}{L}z\right)\exp\left[\mathrm{i}\left(m\theta-\omega t\right)\right],\tag{13}$$

$$j_z(r,\theta,z,t)=\sum_{m,l}j_z^{(l,m)}(r)\cos\left(\frac{l\pi}{L}z\right)\exp\left[\mathrm{i}\left(m\theta-\omega t\right)\right].\tag{14}$$

Therefore, the current density for different types of antennas can be obtained due to the geometry and corresponding Fourier expansion. In order to simplify the Maxwell equations, we introduce the following dimensionless variables:

$$\hat{k}_l=\frac{k_\parallel c}{\omega}=\frac{l\pi c}{L\omega},\quad \hat{r}=\frac{r\omega}{c},$$
$$\hat{\boldsymbol{B}}=\frac{\boldsymbol{B}r_a}{\mu_0 I_a},\quad \hat{\boldsymbol{E}}=\frac{\boldsymbol{E}r_a}{\mu_0 I_a c},\quad \hat{\boldsymbol{j}}_a=\frac{\boldsymbol{j}_a r_a c}{I_a\omega}$$

and phase modified fields

$$E_\phi=-\mathrm{i}E_\theta,\quad B_\phi=\mathrm{i}B_\theta.$$

Using these relations, Eqs. (2) and (3) can be expanded to the four differential equations for each (l,m) mode:

$$\frac{\mathrm{d}\hat{E}_\phi}{\mathrm{d}\hat{r}}=\left(\frac{\kappa_2 m}{\kappa_1\hat{r}}-\frac{1}{\hat{r}}\right)\hat{E}_\phi+\frac{\hat{k}_l m}{\kappa_1\hat{r}}\hat{B}_\phi+\left(1-\frac{m^2}{\hat{r}^2\kappa_1}\right)\hat{B}_z,\tag{15}$$

$$\frac{\mathrm{d}\hat{E}_z}{\mathrm{d}\hat{r}}=\frac{\kappa_2\hat{k}_l}{\kappa_1}\hat{E}_\phi+\left(\frac{\hat{k}_l^2}{\kappa_1}-1\right)\hat{B}_\phi-\frac{\hat{k}_l m}{\kappa_1\hat{r}}\hat{B}_z,\tag{16}$$

$$\frac{\mathrm{d}\hat{B}_\phi}{\mathrm{d}\hat{r}}=\frac{m\hat{k}_l}{\hat{r}}\hat{E}_\phi+\left(\kappa_3-\frac{m^2}{r^2}\right)\hat{E}_z-\frac{1}{\hat{r}}\hat{B}_\phi,\tag{17}$$

$$\begin{aligned}\frac{\mathrm{d}\hat{B}_z}{\mathrm{d}\hat{r}}&=\left(\frac{\kappa_2^2}{\kappa_1}+\hat{k}_l^2-\kappa_1\right)\hat{E}_\phi-\frac{m\hat{k}_l}{\hat{r}}\hat{E}_z\\&\quad+\frac{\kappa_2\hat{k}_l}{\kappa_1}\hat{B}_\phi-\frac{\kappa_2 m}{\kappa_1\hat{r}}\hat{B}_z,\end{aligned}\tag{18}$$

and the two algebraic equations:

$$\hat{E}_r=\frac{\kappa_2}{\kappa_1}\hat{E}_\phi+\frac{\hat{k}_l}{\kappa_1}\hat{B}_\phi-\frac{m}{\hat{r}\kappa_1}\hat{B}_z,\tag{19}$$

$$\hat{B}_r=\frac{m}{\hat{r}}\hat{E}_z-\hat{k}_l\hat{E}_\phi.\tag{20}$$

Thus, this equation system has been simplified to an ordinary differential problem. Considering different situations of plasmas, the methods for obtained solutions are distinct. In radially uniform plasmas, the solutions of this equation system can be obtained analytically. All EM field components can be expressed as the combination of Bessel functions or modified Bessel functions.[22] In non-uniform plasma density case, the equations system has to be solved numerically. The 4- and 5-th order Runge–Kuta method is applied to obtain the solutions. This cylindrical 1D plasma–wave model has been introduced by researchers and verified by comparing with the experiments.[20,23,24]

2.3. Power deposition in the plasma

Once all EM fields are obtained, the power absorption by plasmas is taken into account. In this work, the helicon plasma has a high plasma density and relatively low electron temperature. Therefore, the collisional damping is considered as the main mechanism of wave dissipation and neglects the kinetic effects, such as Landau damping.[25] In our 1D wave model, it is assumed that the antenna wire is a perfect conductor and no power loss occurs inside the antenna.[26,27] Thus, all power emitted by the antenna is absorbed in the plasma column. Then, the time-averaged power density absorbed by the plasma at a given location (r,θ,z) is[20]

$$p_{\mathrm{abs}}=\frac{1}{2}\mathrm{Re}\left(\boldsymbol{E}^*\cdot\boldsymbol{j}\right)=\frac{1}{2}\mathrm{Re}\left(\boldsymbol{E}^*\cdot\bar{\bar{\sigma}}\cdot\boldsymbol{E}\right),\tag{21}$$

where $\bar{\bar{\sigma}}=-\mathrm{i}\omega\bar{\bar{\varepsilon}}$ is the plasma conductivity tensor. The fields $\boldsymbol{E}$ are the sum of all (l,m) modes. Next, averaging over z and θ, the radial distribution of power density can be defined as

$$P_{\mathrm{abs}}(r)=\int_0^{2\pi}\int_0^L p_{\mathrm{abs}}(r,\theta,z)\,\mathrm{d}\theta\,\mathrm{d}z.\tag{22}$$

Then, the total absorbed power P_{total} is the integration of the whole plasma volume

$$P_{\text{total}} = \int_0^{r_p} P_{\text{abs}}(r) \cdot r \, \mathrm{d}r. \tag{23}$$

Therefore, according to Joule's law, the plasma resistance R is given as

$$R = \frac{2P_{\text{total}}}{I_a^2}. \tag{24}$$

The plasma resistance is used to evaluate the performance of the RF antenna coupling with the plasma column.

3. Results and discussion

With the purpose of studying the plasma–wave interaction near the lower hybrid frequency, simulations are based on a typical geometry of the helicon source.[28] The gas is argon, the radially cold, uniform plasma and axial static magnetic field are taken into account. The half-turn helical antenna, which has been widely used in laboratory, is applied in simulations. The expression of the current density is written as a function of the (l,m) modes.[29,30] The validation and convergence of the (l,m) modes have been carried out in a large range of (l,m) mode with $m = [-151, 151]$ and $l = [1, 200]$. The $l = [1, 30]$ and $m = [-9, 9]$ are selected to ensure that the convergence of (l,m) mode is achieved. In addition, only odd number of m modes for the helical antenna is excited in terms of the geometry of the antenna.[31] Then, the main parameters are summarized in Table 1. These parameters are used in all calculations, except for the one whose variation is being studied.

Table 1. Summary of input data for the plasma–wave interaction simulations.

Parameter		Value
r_p	Plasma radius	0.0735 m
L	Plasma and cage axial length	$5r_p$
r_w	External cage radius	$2r_p$
B_0	Applied magnetic field	450 G
T_e	Electron temperature	20 eV
n_0	Plasma density	5.6×10^{18} m^{-3}
ν_e	Electron collision frequency	3.26 MHz
f_0	Frequency of the RF emission	13.56 MHz
r_a	Antenna loop radius	$1.05r_p$
L_a	Antenna axial length	$0.4L$
z_a	Antenna symmetry plane	$L/3$

3.1. Wave propagation and power deposition

In this subsection, the investigation of the wave propagation and power deposition near the lower hybrid frequency is carried out. We first discuss the feature of the wave propagation according to the dispersion relation.

Figure 1 gives the relation between ω_{ce}/ω and $k_\perp d_e$ calculated by Eq. (8). It shows the perpendicular wavenumber as a function of the ratio ω_{ce}/ω at a fixed plasma density. The parallel wavenumber $k_\parallel = 17.1$ ($l = 2$) is selected, and the corresponding dimensionless parameter $k_\parallel d_e$ is 0.0384. The collision and collisionless cases are also considered. In the collisionless case, there are two roots for $k_\perp$, representing the helicon wave and the TG wave.[32] At low values of ω_{ce}/ω, it is seen that there is no real solution for $k_\perp$. It illustrates that no wave propagates in this regime. With ω_{ce}/ω increasing, two kinds of waves, helicon mode and TG mode, propagate. The value of the wavenumber of two waves is close at the beginning and then TG mode goes up rapidly and has a much larger $k_\perp$ than the helicon mode. As the ratio ω_{ce}/ω continues to increase, the perpendicular wavenumber $k_\perp$ for the slow wave (TG wave) tends to be infinite when $\omega = \omega_{lh}$ and $k_\perp$ of the fast wave (HE wave) becomes very small. This means that the resonance will occur near the lower hybrid frequency and the power absorption in plasmas is expected to have a local maximum when ω is close to ω_{lh}.

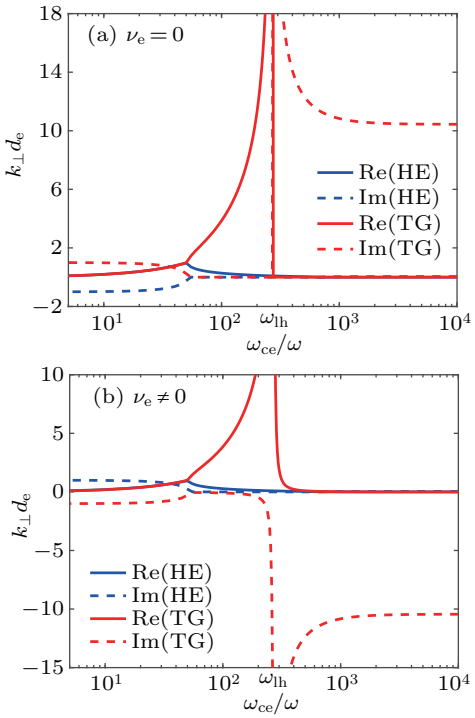


Fig. 1. The perpendicular wavenumber $k_\perp$ versus the ratio ω_{ce}/ω. The plasma density is 5.6×10^{18} m^{-3}; the parallel wavenumbers $k_\parallel$ is 17.1 m^{-1} and the corresponding dimensionless parameter $k_\parallel d_e$ is 0.0384. In the collisional case, the electron collision frequency ν_e is 3.26 MHz. The blue lines represent the helicon wave and the red lines stand for the TG wave. The solid and dashed lines represent the real and imaginary parts, respectively. The magnitude of TG wavenumber is too large to display with the given scale near the region where $\omega \sim \omega_{lh}$.

For the collisional case, the basic trend is consistent with the collisionless case and there are some differences caused by ν_e. The sign of imaginary part of two waves is changed. This is because the collision frequency is the damping rate in the dielectric tensor and contributes to the imaginary part. In addition, there is a knee in the profile of TG mode near the lower

hybrid frequency, and it does not becomes zero suddenly like the collisionless case. This may cause the resonance to change slightly near the lower hybrid frequency and can be used to explain the frequency shift in the experiments.[8]

Based on the analysis of the dispersion relation, the distribution of wave fields and the corresponding power density near the lower hybrid frequency is given in Figs. 2 and 3, respectively. The magnetic field is $B_0 = 2000$ G and the value of $\omega_{\rm lh}/\omega$ is 1.53. It is shown that the wave fields in the bulk region of the plasma is small and only has a large amplitude near the boundary. This phenomenon is consistent with the results of the wavenumber given in Fig. 1. When the frequency ω is close to $\omega_{\rm lh}$, the wavenumber of helicon mode becomes zero and TG mode tends to be infinite. Therefore, the wave can hardly propagate in the center of the plasma and is only damped quickly near the boundary. The radial power density shown in Fig. 3 further confirms this conclusion. The power deposition in the bulk region of the plasma is trivial and the main contribution concentrates in a very thin layer near the boundary. This also provides the evidence of the resonance when ω reaches $\omega_{\rm lh}$.

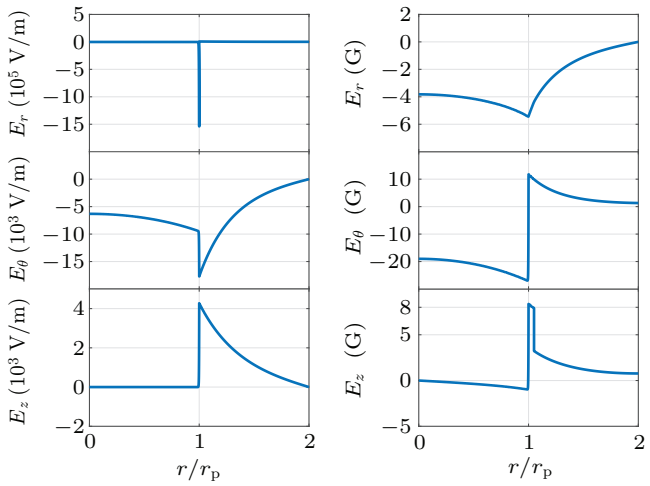


Fig. 2. Radial profiles of electromagnetic fields at $\theta = 0$, $z = L/4$, $B_0 = 2000$ G, $n_0 = 5.6 \times 10^{18}$ m^{-3} and $I_0 = 15$ A.

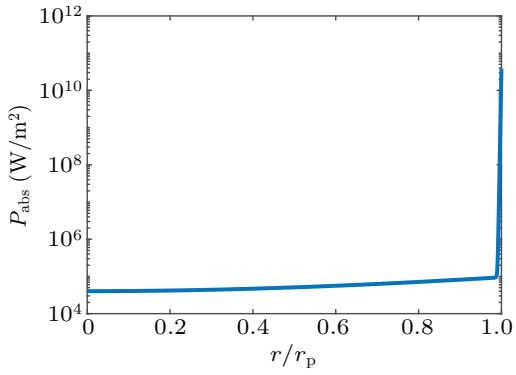


Fig. 3. Power absorption distribution in the radial direction for the case of Fig. 2.

3.2. Parametric investigation

In this subsection, the parametric investigation of the power deposition near the lower hybrid frequency is achieved. The influences of the RF frequency, applied magnetic fields and the plasma density on the power deposition are analyzed.

Figure 4 shows the plasma resistance versus the magnetic field for different l modes and plasma densities, and the RF frequency is fixed. As is seen, the resistance when $\omega < \omega_{\rm lh}$ has numerous local peaks in the regime of two waves propagating. Then, when the lower hybrid frequency is near the wave frequency, the plasma resistance presents few sharp peaks. This can be explained by the existing eigenmodes near $\omega_{\rm lh}$ proposed by Cho.[13] For $l = 2$ the resistance is up to 15.08 Ω. However, for different l modes, the peak location changes with the magnetic field and the plasma density. It can be explained by the dispersion relation of Eq. (8). The perpendicular wavenumber is effected by the B_0 and n_0 and leads to the variation of the eigenmodes. Therefore, the corresponding local peak varies.

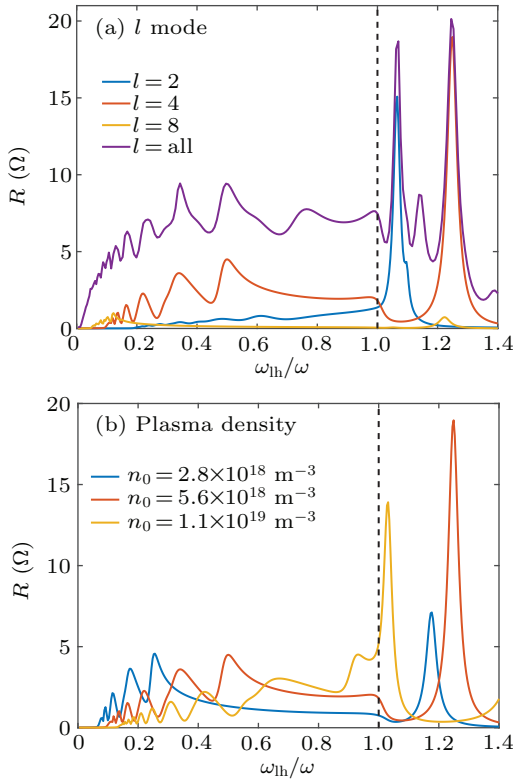


Fig. 4. Resistance profiles varying with the ratio $\omega_{\rm lh}/\omega$. The RF frequency is fixed at 13.56 MHz. The magnetic field is varied. (a) The case for different l modes, with the plasma density 5.6×10^{18} m^{-3}. (b) The results for different plasma densities with $l = 4$.

Figure 5 represents the 2D color maps of resistance varying with the magnetic field and plasma density. The different wave propagation regimes are separated by the dashed line, and the solid lines are the separatrix of the lower hybrid frequency. Below the red solid line, we can see numerous local peaks in the two wave propagating regimes. The linear relation

between the magnetic field and plasma density for the plasma resistance is achieved. This can be explained by the dispersion relation of helicon plasmas[22,33] and has been confirmed in the experiments.[32,34]

Near the lower hybrid resonance, several isolated peaks of resistance emerge and the linear relation between the magnetic field and plasma density for the local peaks still holds. There is a transition near the lower hybrid frequency. The linear slope for the peaks is changed and the values of these peaks are much higher than the peaks below the separatrix, because of the resonance. Near the lower hybrid frequency, the perpendicular wavenumber of TG wave goes to infinity. The resonance dominates the behavior of wave propagation. Hence, the larger power deposition is achieved. In Fig. 5(d), all l modes are taken into account. More local peaks lie in the regime above the red line. This also confirms that the resonance is the main mechanism of the power deposition for helicon plasmas when ω is near $\omega_{\rm lh}$.

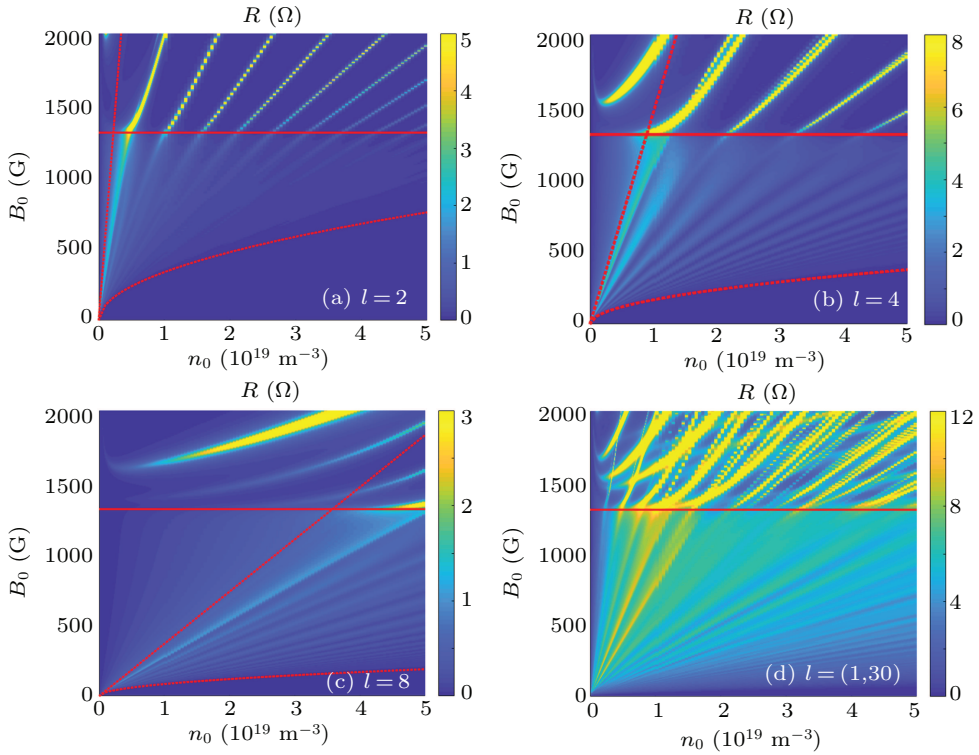


Fig. 5. The 2D color map of resistance varying with both the magnetic field and plasma density for different l modes. The red dashed line represents the different wave propagation regimes and the red solid line is the separatrix of the lower hybrid frequency.

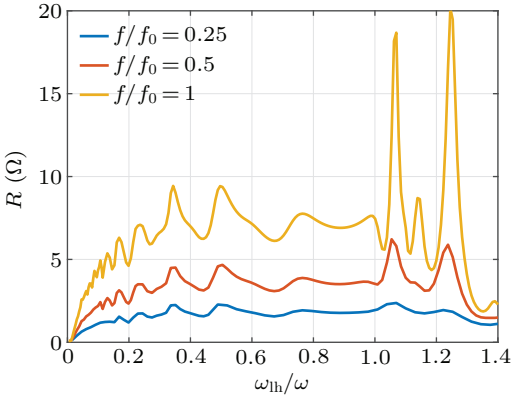


Fig. 6. Plasma resistance versus magnetic field and wave frequency. The resistance is as a function of magnetic field with different frequencies. The nominal frequency f_0 is 13.56 MHz.

Figure 6 gives the resistance for different RF frequency as a function of magnetic fields. All l modes are taken into account. The local peaks appear in the case of $\omega < \omega_{\rm lh}$. The higher applied frequency is applied, the higher resistance is achieved, provided that the magnetic field increases proportionally. Near the lower hybrid resonance, there is a larger local peak of the resistance. This keeps consistence with the previous results. Additionally, we can observe the monotonic dependence of the resistance with the antenna frequency in terms of Eq. (21). At a fixed $\omega_{\rm lh}/\omega$, the power absorption is larger when the emission frequency is increasing.

4. Conclusion

The (0D) dispersion relation and the 1D radially plasma–wave interaction model have been established to investigate the characteristics of the plasma–wave interaction near the lower hybrid frequency. The wave propagation near the lower hybrid frequency are described according to the dispersion relation of helicon plasmas. The power deposition mainly concentrates on a thin layer near the boundary. Furthermore, the parametric investigation is illustrated. When the frequency is near the lower hybrid frequency, the plasma resistance can reach a local peak because of the lower hybrid resonance.

The resonance is effected by the plasma density and parallel wavenumber and leads to the frequency shifting of the local peak. The linear relation between the magnetic field and the plasma density is still satisfied but a transition leads to a change of slope. The plasma resistance is increasing when the emission frequency is larger and the relation between the frequency and magnetic field is linear.

Acknowledgements

Project supported by the Open Fund for Science and Technology on Vacuum Technology and Physics Laboratory, Lanzhou Institute of Physics (Grant No. ZWK1703). The authors also acknowledge the support of the National Natural Science Foundation of China (Grant No. 51907039) and Shenzhen Technology Project (Grant Nos. JCYJ20190806142603534 and ZDSYS201707280904031). The contribution of E. Ahedo and M. Merino has been supported by the ESPEOS project (Grant No. PID2019-108034RB-I00/AEI/10.13039/501100011033), funded by the Agencia Estatal de Investigación (Spanish National Research Agency).

References

[1] Nicholas A K and Paulett C L 1971 *Phys. Rev. A* **4** 2094
[2] Huba J D and Wu C S 1976 *Phys. Fluids* **19** 988
[3] Norgren C 2011 *Lower hybrid drift wave properties in space plasma* (Master thesis) (Sweden: Uppsala University)
[4] Xiao F L, Yang C, Su Z P, Zhou Q H, He Z G, He Y H Baker D N, Spence H E, Funsten H O and Blake J B 2015 *Nat. Commun.* **6** 8590
[5] Yang C, Su Z P, Xiao F L, Zheng H N, Wang Y M, Wang S, Spence H E, Reeves G D, Baker D N and Blake J B 2017 *Geophys. Res. Lett.* **44** 3980
[6] Boswell R W 1984 *Plasma Phys. Control Fusion* **26** 1147
[7] Zhu P Y and Boswell R W 1989 *Phys. Rev. Lett.* **63** 2805
[8] Yun S M, Kim J H and Chang H Y 1997 *J. Vac. Sci. Technol. A* **15** 673
[9] Cho S W and Swanson D G 1988 *Phys. Fluids* **31** 1123
[10] Balkey M M, Boivin R, Kline J L and Scime E E 2001 *Plasma Sources Sci. Technol.* **10** 284
[11] Mori Y, Nakashima H, Baity F W, Goulding R H, Carter M D and Sparks D O 2004 *Plasma Sources Sci. Technol.* **13** 424
[12] Chen F F, Schweickhard E and Goeler V 1985 *Introduction to plasma physics and controlled fusion* Volume 1: *Plasma physics* (Boston: Springer) p. 113
[13] Cho S W 2000 *Phys. Plasmas* **7** 417
[14] Yun S M and Chang H Y 1997 *Phys. Lett. A* **248** 400
[15] Kwak J G, Kim S K and Cho S W 2000 *Phys. Lett. A* **267** 384
[16] Scime E E, Keiter P A, Balker M M, Kline J L, Sun X, Keesee A M, Hardin R A, Biloiu I A, Houshmandyar S and Thakur S C 2015 *J. Plasma Phys.* **81** 345810103
[17] Buttenschon B, Fahrenkamp N and Grulke O 2018 *Plasma Phys. Control Fusion* **60** 075005
[18] Lieberman M A and Lichtenberg A J 2005 *Principles of plasma discharges and materials processing* (Chichester: John Wiley & Sons) p. 112
[19] Shamrai K P and Taranov V B 1996 *Plasma Sources Sci. Technol.* **5** 474
[20] Cho S W 1996 *Phys. Plasmas* **3** 4268
[21] Ahedo E 2011 *Plasma Phys. Control Fusion* **53** 124037
[22] Shamrai K P and Taranov V B 1994 *Plasma Phys. Control Fusion* **36** 1719
[23] Chen F F and Arnush D 1997 *Phys. Plasmas* **4** 3411
[24] Arnush D and Chen F F 1998 *Phys. Plasmas* **5** 1239
[25] Chen F F and Blackwell D D 1999 *Phys. Rev. Lett.* **82** 2677
[26] Shamrai K P, Pavlenko V P and Taranov V B 1997 *Plasma Phys. Control Fusion* **39** 505
[27] Tian B, Merino M and Ahedo E 2018 *Plasma Sources Sci. Technol.* **27** 114003
[28] Navarro J C 2013 *The 33rd International Electric Propulsion Conference*, October 6–10, 2013, Washington, D.C., USA, paper EPC-2013-285
[29] Chen G Y, Arefiev Alexey V, Bengtson R D, Breizman B N, Lee C A and Raja L L 2006 *Phys. Plasmas* **13** 123507
[30] Tian B 2015 *The 34rd International Electric Propulsion Conference*, July 4–10, 2015, Hyogo-Kobe, Japan, paper IEPC-2015-326/ISTS-2015-B-326
[31] Chen F F 2015 *Plasma Sources Sci. Technol.* **24** 014001
[32] Chen F F and Boswell R W 1997 *IEEE T. Plasma Sci.* **25** 1245
[33] Chen F F 1991 *Plasma Phys. Control Fusion* **33** 339
[34] Lafleur T, Charles C and Boswell R W 2011 *J. Phys. D: Appl. Phys.* **44** 055202